International Journal of Hydrogen Energy 88 (2024) 1463–1473

Contents lists available at ScienceDirect

International Journal of Hydrogen Energy

journal homepage: www.elsevier.com/locate/he

An experimental study of hydrogen sorption and permeation in high-performance polyamides

Lorenzo Merlonghi [a,c], Omar Atiq [a,c], Riccardo Rea [b], Enzo Mangano [b], Alexander Stroeks [d], Marco Giacinti Baschetti [a,c], Maria Grazia De Angelis [b,c,*]

[a] Department of Civil, Chemical, Environmental and Material Engineering, (DICAM), Alma Mater Studiorum – Università di Bologna, Via Terracini 28, 40131, Bologna, Italy
[b] Institute for Materials and Processes, School of Engineering, University of Edinburgh, Sanderson Building, Robert Stevenson Road, EH9 3FB, Scotland, UK
[c] DPI, P.O. Box 902, 5600 AX, Eindhoven, the Netherlands
[d] Envalior, DSM Engineering Materials, Urmonderbaan 22, 6167 RD Geleen, P.O. Box 1077, 6160 BB, Geleen, the Netherlands

A B S T R A C T

Semicrystalline polyamides (PAs) are optimal materials to develop high-pressure resistant liners for type IV hydrogen storage tanks due to a favorable combination of barrier performance, mechanical resistance, and lightness. However, experimental data on hydrogen transport in PAs are incomplete or inconsistent, and usually do not report separately the contributions of solubility and diffusivity, hence limiting a deep understanding of the permeation mechanism and its dependence on the material structure. Moreover, recent developments have led to the design of modified polyamides which could better serve the high-pressure storage applications. In this work, the hydrogen barrier performance of Polyamide 6 (PA6), Polyamide 11 (PA11) and an impact-modified PA 6 (PA6-I), was evaluated and the results obtained with different techniques and on different samples compared. Permeation measurements were performed in constant-volume and constant-pressure apparatuses at different temperatures and pressures, on different samples of each material. Sorption measurements were carried out into a differential sorption system. Results from the permeation and sorption devices were compared against each other and with literature data, allowing to understand the effect of various factors. The H_2 solubility in PA is mostly affected by density, as a lower free volume of the amorphous phase leads to a lower gas uptake. On the other hand, diffusivity and, consequently, permeability, are also strongly affected by the morphology of the crystal phase, which depends on the production protocol. In most of the cases inspected, the discrepancy between data from different experimental techniques or literature works can be explained by the different crystal morphology of the samples used in the test. Temperature enhances diffusivity, permeability and solubility, while the pressure reduces the permeability, as it lowers the free volume, and increases the activation energy of permeation. An estimation of the minimum thickness required to meet high-pressure storage technical guidelines was provided for the case of PA6-I.

1. Introduction

The evolution of the conceptual design of high pressure hydrogen storage tanks has seen the phasing out of metal liners (types-I,II,III), due to the relative high reservoir weight and the material embrittlement [1,2] and the breakthrough of type IV tanks which consists of two parts: a full thermoplastic liner and a polymer-based composite shell. The composite might be based on continuous glass or carbon fibers embedded in an epoxy matrix and provides sufficient mechanical strength to withstand the high operating pressures and sudden impact incidents. The liner contributes to safety by providing sufficient hydrogen gas barrier and blistering performance [3]. In the most recent type-V tank, the liner is eliminated and the storage system consists only of a composite material, acting also as a gas barrier. Furthermore, the type-V tank allows for a 20% weight reduction of the reservoir and eliminates the issue of stress compatibility between the polymer liner and the composite shell. However, it has a limited hydrogen barrier performance which limits its use to medium pressure applications (up to 350 bar) [4]. Therefore, type-IV tanks currently represents the state of the art for high pressure storage (700 bar) [5].

The most stringent case for the permeation rate, according to the European normative (EU No 406/2010) is the “large car” scenario which defines a maximum hydrogen leak rate per tank unit volume (liquid water capacity) of 6 cm^3_{STP}/(h L) [6,7] To meet such requirements, industries have explored semi-crystalline polymers such as high-density polyethylene (HDPE) and polyamides (PAs) [8,9]. As an example, QUANTUM (USA) has developed and commercialised type IV ‘Q-lite’ storage tanks made of a cross-linked polyethylene liner with a carbon

* Corresponding author. Institute for Materials and Processes, School of Engineering, University of Edinburgh, Sanderson Building, Robert Stevenson Road, EH9 3FB, Scotland, UK.
E-mail address: grazia.deangelis@ed.ac.uk (M.G. De Angelis).

https://doi.org/10.1016/j.ijhydene.2024.09.053
Received 21 March 2024; Received in revised form 2 September 2024; Accepted 4 September 2024
Available online 5 October 2024

fiber overwrap [10]. Toyota (Japan) released high-pressure hydrogen tanks which employ a liner made of high-strength Nylon 6 [11]. Similar solutions were adopted by Hexagon (Norway), Faurecia (France) and Luxfer (USA) [12–14]. Although the use of semi-crystalline polymer liners is already a reality, hydrogen barrier data in such materials are scarce in the literature, and there is the need for a more thorough material characterization, addressed at the identification of the best performing candidates in various operating conditions and the development of reliable structure-property correlations for fast material design.

The gas permeability in semi-crystalline polymers, which is commonly described according to the solution-diffusion model [15], is strongly dependent on their complex biphasic morphology. The overall barrier performance of the materials, indeed, is determined by the concurrent contributions of the two phases, namely, the amorphous one, whose properties are related to the phase density and chain mobility, and the crystalline one, which is impermeable but affects permeabiity to an extent that depends on its relative content, morphology and distribution [16–21].

Polyamides have a better barrier performance compared to polyethylenes, despite their lower degree of crystallinity [22,23]. Such a result highlights the non-trivial behavior of semicrystalline polymers, and the key contribution of the amorphous phase, which is denser and less permeable, to the overall barrier performance.

Different methods can be used to measure gas permeability and diffusivity in polymeric films or sheets, but the two main ones are the time-lag and the constant-flux method [24]. The first one consists of measuring the number of moles which pass through the sample, which can be done by monitoring the increase in the downstream pressure at constant volume [25] or the increase in the downstream volume at constant pressure [26], with time. The second method consists in measuring the gas flux during time, e.g. by sweeping the downstream side with another gas, usually inert, and measuring its concentration with a gas detector, such as a mass spectrometer [8,9,22,23].

Using the constant-volume time-lag method, Humpenoder [23] measured hydrogen permeability and diffusivity in an undefined polyamide between −10 and 30 °C. Picard et al. [27] investigated the effect of inorganic particles in polyamide 6 (PA6), at 20 °C and 3 bar while Sun et al. [9] extended the analysis to a wider range of temperatures (up to 85 °C) and pressures (up to 500 bar). In addition, Kanesugi et al. [22] measured H_2 permeability and diffusivity in PA6, polyamide 11 (PA11) and polyamide 12 (PA12) at 30 °C and 6 bar and extended the testing of PA11 to high pressures (900 bar). Ash et al. [28] measured vacuum permeability and diffusivity of H_2 in PA11 at different temperatures (20–60 °C). Dong et al. [25] measured the variation of H_2 permeability in PA6 with temperature (35–85 °C) and pressure (150–900 bar) while Smith et al. [29] explored the same property in a wider range of temperatures, from −30 to 85 °C, at 137 bar. The modification of PA6 was investigated by Wolter et al. [26], who measured the permeability of H_2 in PA6 pristine and modified with carbon fibers (PA6-CF) at 100 bar and 55 °C using the constant-pressure time-lag method.

For the direct determination of gas solubility in barrier polymers, the most common approach is the one through which the mass gained/loss by the material during adsorption/desorption is calculated from the decrease/increase of the pressure in the dead volume of the cell in which the sample is placed. The gravimetric methods are not appropriate to measure low solubility, especially for light gases such as hydrogen. As a result, direct sorption data in polyamides are scarce in the literature. To our knowledge, the only direct measurement of hydrogen sorption in polyamides was performed by Ash et al. on PA11 in 1970 at different temperatures (20–60 °C) but at very low pressure [28]: such data were compared with the indirect measurement of the sorption coefficient from permeation tests, highlighting a discrepancy between the two approaches. However, direct sorption data in other polyamides, such as PA6, and at higher pressures are still lacking.

This brief literature survey shows that the various literature references report very different transport coefficients for the same materials, which could be due to the different methods used to measure them, or to differences in the microstructure. To clarify this aspect, in this work we performed a comprehensive experimental analysis of hydrogen permeation, diffusion, and sorption in a series of polyamides using different measurement techniques, with the aim of identifying and addressing the deviations between results coming from different test methods. Furthermore, in addition to standard PA11 and PA6 samples analyzed in other literature sources, we tested the barrier performance of an impact-modified polyamide 6 (PA6I), for which hydrogen transport data were obtained in this work for the first time. PA6I has better impact resistance compared to PA6 due to the presence of a dispersed rubbery phase which provides the polymer with an increased ability to adsorb and/or dissipate the energy of impacts [30]. This material, however, differs significantly with other modified types of PA6, e.g. the one containing carbon fibers explored by Wolter et al. [26].

Hydrogen permeation, diffusion, and sorption coefficients were evaluated in various pressure and temperature conditions using different techniques and apparatuses: a constant-volume permeation rig available at the University of Bologna (UniBo), a constant-pressure, high-pressure permeation apparatus (TesTneT Engineering GmbH) and a constant-volume adsorption differential volumetric apparatus (ADVA) available at University of Edinburgh (UoE). The permeation systems monitor the transient and steady state permeation across a polymer film subject to a gas pressure gradient, allowing to directly estimate the permeability and the diffusivity via the time-lag method. The sorption device measures the gas uptake in a polymer sample (e.g. film, pellet, powder) subject to a spatially uniform gas pressure, as a function of time. Data at equilibrium provide the solubility of the gas in the polymer at the final equilibrium pressure, while the transient behavior can be elaborated knowing the geometry of the sample to obtain the diffusivity. The results from the two experimental devices allow to gain understanding on the separate contributions of sorption and diffusion and can be compared to check for consistency and assess the validity of the solution-diffusion model described below. The values were also related to the structural properties of the material, such as density and crystallinity, to better understand the hydrogen transport in PA polymers.

2. Materials and methods

2.1. Theoretical background

Considering a dense polymer film with thickness L subject to a gas pressure difference Δp between the upstream high pressure p^{up} and the downstream low pressure p^{dw}, the gas flux across the membrane at steady state can be expressed as:

$$J = P \frac{\Delta p}{L} = P \frac{p^{up} - p^{dw}}{L} \quad \text{Eq. (1)}$$

where P is the permeability of the gas in the material. The gas transport through a homogeneous film occurs by dissolution on the high-pressure side of the sample, diffusion of the gas molecules through it and gas desorption on the low-pressure side. Therefore, if diffusion follows Fick's law and the solubility of the gas in the membrane is related to its pressure in the gas phase through the solubility coefficient S, i.e., if the solution-diffusion model is valid, it is possible to evaluate the permeability as the product of diffusivity D and solubility S [15]:

$$P = S\,D \quad \text{Eq. (2)}$$

In order to reduce the flux across the liner material at fixed pressure difference Δp between the inner core and the ambient, it is required to increase the thickness L, increasing weight and costs, or reduce P, by choosing a material with lower S and/or D. Generally P, D and S of gases in semicrystalline polymers depend on pressure p and temperature T. However, the pressure dependency can be neglected at low pressures,

from 1 to 10 bar, while the temperature dependency of P, D and S can be expressed by using the Arrhenius law:

$$P = P_0 \exp\left(-\frac{E_P}{RT}\right) \quad \text{Eq. (3)}$$

$$D = D_0 \exp\left(-\frac{E_D}{RT}\right) \quad \text{Eq. (4)}$$

$$S = S_0 \exp\left(-\frac{\Delta H_S}{RT}\right) \quad \text{Eq. (5)}$$

Where R is the gas constant, P_o, D_o and S_o are the limit values of the three pre-exponential factors, and E_P is the activation energy for the permeation, which, due to Eq. [2], is the sum of the activation energy of the diffusion process E_D and the enthalpy of solution ΔH_S.

2.2. Materials

Different polyamide samples were provided by *Envalior*, Geleen, NL. The impact-modified polyamide 6 was supplied as 2 mm slabs while Polyamide 11 in the form of pellets with average equivalent radius of 1.55 mm. Finally, PA6 was provided in the form of slabs (2 mm) and pellets with an average equivalent radius of 1.25 mm. The PA6 and PA6I slabs were produced through injection molding with a typical melting temperature of 250 °C and a mold temperature of T = 70 °C then promptly packed in alumina bags to prevent moisture absorption.

The high-pressure permeation experiments on PA6 and PA6I slabs and the sorption tests on PA6 and PA11 pellets were carried out on the samples as supplied. On the other hand, for the low-pressure permeation tests the pristine materials were processed into thin film membranes following a series of steps. The PA6 slabs were cut into pieces and subsequently dissolved in formic acid at 70 °C. The solution was then cast on a Petri dish to obtain flat films with a thickness around 50 μm. A dense membrane of 230 μm was finally obtained by stacking and hot-pressing at 250 °C several single films using a Carver Model C Laboratory Press (Clamping Force: 12 tons; Platens: 15.2 cm × 15.2 cm). The temperature ramp and the applied force were tuned to prevent the thermomechanical degradation of the material through a trial-and-error procedure aimed at obtaining dense and flat membranes. Similarly, PA11 pellets were dissolved in a formic acid and dichloromethane solution (1:1 vol) at 70 °C and cast into flat films of 50 μm. Finally, a 200 μm thick membrane was obtained from a series of films hot-pressed at 210 °C. PA6I slabs were directly hot-pressed at 250 °C to obtain a 700 μm membrane; in this case, indeed, the dissolution was avoided to preserve the properties of the material, i.e., the chemical stability of the impact modifier.

2.3. Density and crystallinity

The samples were characterized in terms of crystallinity and density, properties that are well-known to dictate the overall barrier performance of the polymer. The mass degree of crystallinity, X_{cr}, was measured using a differential scanning calorimeter (DSC) equipment (TA instruments - DSC Q10). The analyses were carried out on the pristine materials as well as on the newly prepared thin membranes. Ten milligrams of each sample were tested under a nitrogen flow rate of 20 mL/min from −50 °C up to 270 °C setting a heating ramp of 10 °C/min. The heat of melting, ΔH_m, was estimated as the integral of the heat absorbed as a function of temperature; ultimately, X_{cr} was assessed from the heat of melting of the fully crystalline material ΔH_{cr} (230 J/g for PA6 and PA6I [31,32]and 189 J/g for PA11 [33]).

$$X_{cr} = \frac{\Delta H_m}{\Delta H_{cr}} \quad \text{Eq. (6)}$$

The overall density of slabs and pellet, which correspond to the semi-crystalline density, ρ_{sc}, was measured using a pycnometer with a calibrated volume using acetone as immersion fluid [34]. Moreover, the density of the pellets was measured directly inside the sorption apparatus through fast helium expansions at 1 bar and 25 °C, to check for consistency with the pycnometer technique.

The density of the thin membranes could not be evaluated using this method, due to their high surface area and the negligible weight. Combining the value of the mass degree of crystallinity with the semi-crystalline density ρ_{sc} and the crystal density, ρ_{cr}, the volume degree of crystallinity Φ_{c_r} was evaluated according to the following relation:

$$\phi_{cr} = X_{cr}\frac{\rho_{sc}}{\rho_{cr}} \quad \text{Eq. (7)}$$

In this framework, the value of the crystalline density of PA6 estimated from X-ray analysis was found to be equal to 1.23 g/cm^3 [35] whereas PA11 crystal density was evaluated using the following empirical relation [35]:

$$\rho_{cr} = \frac{M_u}{1.435\ V_w} \quad \text{Eq. (8)}$$

where V_w is the van der Waals volume equal to 115.3 cm^3/mol and M_u is the molar mass of the repeating unit of PA11, equal to 183.3 g/mol [35]. The estimated value, equal to 1.108 g/cm^3, closely matches the one reported by other authors (1.10 g/cm^3) [36].

As commonly assumed, hydrogen molecules do not sorb into the densely packed crystalline domains, therefore, the volumetric properties of the confined amorphous phase fraction are expected to have a major role in determining the overall uptake. The constrained amorphous phase density, ρ_{ca}, was estimated as:

$$\rho_{ca} = \frac{\rho_{sc} - \phi_{cr}\rho_{cr}}{(1 - \phi_{cr})} \quad \text{Eq. (9)}$$

The latter value was finally compared to the free amorphous density, ρ_{fa}, of PA6 and PA11, which corresponds to 1.084 g/cm^3 and 1.01 g/cm^3, respectively [35]. For the sake of completeness, a summary of the mentioned data is reported in the results section (Table 1).

2.4. Low- and high-pressure permeation tests

The gas permeability and diffusivity coefficients in polymeric dense membranes are commonly estimated by means of a manometric permeation experiment (ASTM D1434). In such an apparatus the sample is placed in a permeation cell which separates the upstream and downstream volumes. The sample is supported on a sintered filter in the downstream side, which ensures mechanical resistance towards the upstream pressure and negligible resistance to the gas flux. On the other hand, a Viton rubber O-ring ensures the sealing of the sample on the upstream side. Before the test begins, the leaks in both sides are checked; the system is then put in dynamic vacuum to remove all sorbed gases; finally, it is left in static vacuum, so that the concentration of the gas in the membrane is zero. Once the gas is loaded in the upstream side, a pressure difference Δp is established and the gas molecules start to sorb and diffuse through the material thickness, causing an increase in the downstream pressure until it reaches, at the steady state, a constant increase rate $\left[\frac{dp^{dw}}{dt}\right]_{SS}$, used to calculate the permeability P by means of the following relationship:

$$P = \left[\frac{dp^{dw}}{dt}\right]_{SS} v^{STP}\frac{V^{dw}}{RT}\frac{L}{A\Delta p} \quad \text{Eq. (10)}$$

Where v^{STP} is the standard molar volume, V^{dw} is the downstream volume, A is the permeation area, equal to the area of the sintered filter (Diameter: 15 mm) and L is the thickness, measured using a Mitutoyo micrometer (Precision: 0.001 mm).

From the same test, the diffusion coefficient D is calculated through

Table 1
Tested samples estimated characteristic dimension d, mass degree of crystallinity X_{cr}, semicrystalline density ρ_{sc}, crystalline density ρ_{cr}, volume percent crystallinity Φ_{cr}, constrained amorphous density ρ_{ca} and free amorphous density ρ_{fa}. The values of ρ_{cr} and ρ_{fa} are taken from Ref. [35].

Material	Geometry	d [mm]	X_{cr}	ρ_{sc} [g/cm^3]	ρ_{cr} [g/cm^3]	ϕ_{cr}	ρ_{ca} [g/cm^3]	ρ_{fa} [g/cm^3]
PA6	membrane	0.230	0.24	–	–	–	–	–
PA6I	membrane	0.700	0.24	–	–	–	–	–
PA11	membrane	0.200	0.25	–	–	–	–	–
PA6	slab	2.000	0.28	1.145	1.230	0.26	1.115	1.084
PA6I	slab	2.000	0.21	1.080	1.230	0.18	1.05	1.084
PA6	pellet	1.250	0.25	1.145	1.230	0.23	1.119	1.084
PA11	pellet	1.550	0.25	1.060	1.108	0.23	1.014	1.010

Eq. (11), using the time lag (τ) method [37]:

$$D = \frac{6L^2}{\tau} \qquad \text{Eq. (11)}$$

The set-up of the low-pressure permeation apparatus used in this work is depicted in Fig. 1. The equipment was placed inside a thermostatic chamber with controlled temperature. The system was connected to the hydrogen feeding line (H_2) and to the nitrogen purging line (N_2). Gases with a purity of at least 99.9% were used in the different experimental campaign. Further connections exist with a vacuum Edwards Rotary Pump RV5 (VA) for system evacuation, all vents were collected and sent to a Bunsen (BV) which burnt hydrogen in excess after each experiment. The upstream pressure p^{up} inside the storage tank (ST) was monitored by means of a high-pressure manometer (PU, Druck UNIK 5700) with 0.01 bar accuracy and 0–10000 Torr range, while the downstream pressure p^{dw} was tracked through a low-pressure capacitive manometer (PD, Setra Model 730) having a 0.01 mbar accuracy and 0–100 mbar range. After placing the samples in the permeation cell, dynamic vacuum was kept for at least 12 h to remove all dissolved gases from the polymeric matrix and allow equilibration of system. A leak test followed to ensure the absence of any leakage. Finally, the permeation test was started by loading the upstream side with hydrogen at the desired pressure. The data acquisition was interrupted after 2 h of constant flux at steady state. The tests were repeated twice for each sample and the results averaged.

High-pressure hydrogen diffusion and permeation tests were carried out with TesTneT Engineering GmbH apparatus according to standard ANSI CSA CHMC2. The experimental principle of measuring steady-state permeation and the derivation of diffusivity from non-steady-state permeation data is identical to the low-pressure permeation described above, even if permeation rate is detected with a constant-pressure, rather than a constant-volume, technique. A schematic representation of the high-pressure permeation experimental set-up is provided in Fig. 2 together with a specific display of the hydrogen supply system, the sample and the measuring compartment. In the latter, the amount of hydrogen permeating side is realized by monitoring the position of a marker fluid in a tube, as indicated in the figure [26].

2.5. Sorption tests

Sorption tests on PA11 and PA6 samples were carried out by means of the high-pressure, constant-volume ADVA-270 sorption device [38], presented in Fig. 3, which was validated during the 2020 NIST inter-laboratory study [39]. The system, designed and built at the UoE, shares the same design of the low-pressure ADVA-1, optimized for fast adsorption kinetic measurements up to 1000 Torr [40]. A differential pressure transducer is located between two symmetric and parallel branches which guarantees the same level of accuracy across the whole pressure range investigated. Each side of ADVA-270 has two main volumes connected by a valve. The sample is loaded inside one of the two legs (sample side), while the other one is empty and used as the reference side. The apparatus has an internal volume of about 25 cm^3 per side, can handle a maximum pressure of 276 bar and has three pressure transducers: two for the absolute pressure, located outside the core of the instrument, and one differential sensor. The two absolute sensors have a full-scale reading of 2 and 276 bar respectively and can be swapped to obtain better accuracy in the low-pressure region. The differential transducer is characterized by a full-scale reading of ± 620 mbar and, as the absolute ones, belongs to the Rosemount 3051 series. All the pressure sensors have been calibrated by the manufacturer which guarantees an accuracy of 0.04% of the full-scale reading. The four main volumes of the instrument, V_{DR}/V_{DS} and V_{UR}/V_{US} in Fig. 3, have an

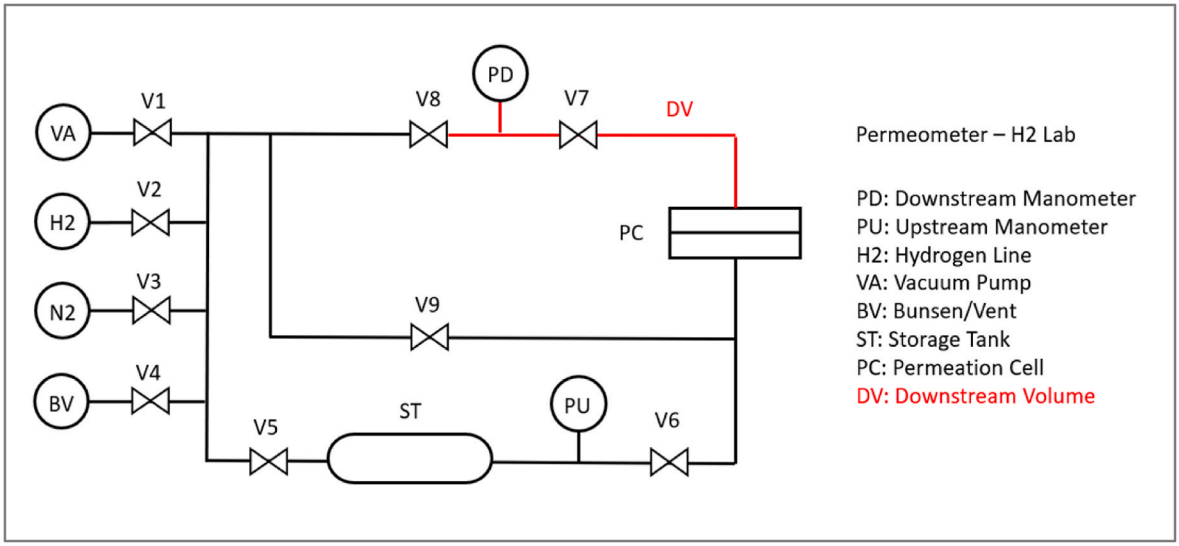

Fig. 1. Schematic representation of UniBo permeation equipment.

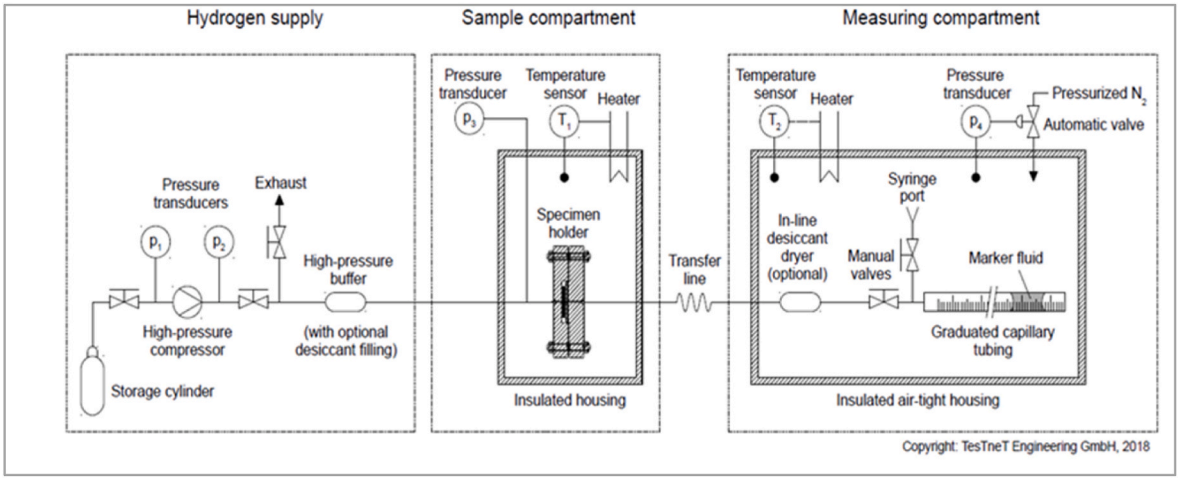

Fig. 2. Schematic representation of TesTneT permeation equipment [26].

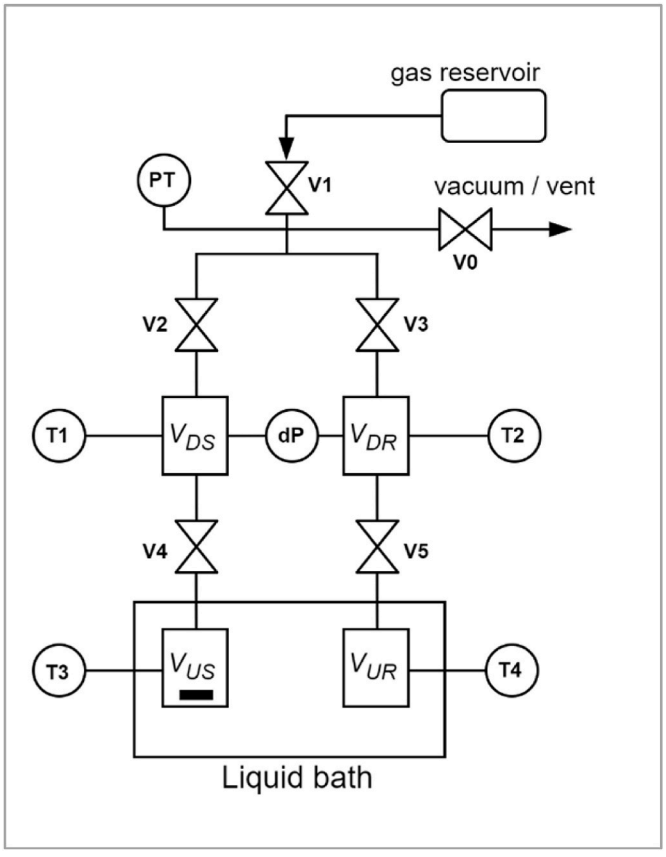

Fig. 3. Schematic representation of ADVA-270 sorption apparatus. PT: absolute pressure transducer (2 or 276 bar), dP: differential pressure transducer. V_{DS},V_{DR}: sample,reference side dosing volume. V_{US},V_{UR}: sample,reference side uptake volume. V2,V3,V4,V5: pneumatic activated bellows valves. V0,V1: manually activated needle valves. The black rectangular stands for the sample placed in V_{US}.

internal K-type thermocouple for the measurement of the temperature. The four valves connecting the dosing and the uptake sections (V2/V3/V4/V5) are pneumatically activated bellows valves (Swagelok HB series). The dosing part of the instrument is exposed to room temperature while the uptake volumes are partially submerged in a recirculating liquid bath served by an external chiller (Julabo CORIO CD-200 F). The presence of a turbopump (Pfeiffer HiCube 80 Eco) and an external furnace allows for the in-situ activation of the sample in high vacuum. Prior to any equilibrium test, the sample (2.52 g for PA11 and 2.05 g for PA6) was loaded and degassed for at least 16 h at 80 °C to ensure the complete removal of any sorbed species. Subsequently, a low-pressure He expansion was performed twice to measure the gas-accessible volume and the volume occupied by the sample. The estimated densities were in satisfactory agreement with the ones estimated through the pycnometer. A blank experiment with He was performed, using the same pressure steps as the ones employed during the H_2 measurements, to verify the zero-adsorption condition in the experimental pressure range. Non-ideality behavior of the gas phase was accounted for by the GERG2008 Equation of State for both He and H_2 [41]. The gases were purchased from BOC having a purity grade of 99.995%.

Once the sample has been regenerated and equilibrated in vacuum at the temperature of the test, the uptake volumes are closed through V4 and V5 and a certain amount of gas is loaded in the dosing volumes, which are then closed by V2 and V3. After this step V4 and V5 are opened, and the gas expands in the uptake volumes and comes in contact with the sample loaded in V_{US}. The gas sorption onto the sample decreases the pressure in V_{US} with respect to V_{UR} thus generating a differential signal which attains a plateau at equilibrium. After that, V4 and V5 are closed again, and the procedure is repeated iteratively. During the isotherm measurements V2/V3 and V4/V5 open and close simultaneously, minimizing the risk of over-pressurization of the differential sensor. The mass balance in the system allows to calculate the molar uptake at each pressure step. Then the solubility coefficient is calculated as the slope of the isotherm, in kg/bar and converted to $cm^3_{STP}/(cm^3\ bar)$ units to compare it with the permeation tests results. The diffusion coefficients from the transient uptake data measured on ADVA-270 were determined using the diffusion model for volumetric systems developed by Brandani [40,42,43]. In its simplest version the model assumes isothermal conditions, linearity within the pressure step, spherical geometry and includes the kinetics of the valve. To avoid the ambiguity in the determination of the initial pressure the raw data are converted to reduced pressure [44], σ_D, through equation 12:

$$\sigma_D = \frac{p_D(t) - p_\infty}{p_D^0 - p_\infty} \qquad \text{Eq. (12)}$$

Where $p_D(t)$is the pressure measured in the dosing cell of the sample branch as function of time, p_D^0 its value at time 0 (before the gas expansion) and p_∞ is the final pressure at equilibrium.

3. Results and discussion

3.1. Density and crystallinity

The density and crystallinity measurements carried out on the pristine slabs and pellets are reported in Table 1, together with the characteristic dimension *d*, equal to the thickness for the membranes/slabs and the equivalent radius for pellets.

It can be noticed that PA6 exhibits higher amorphous and crystal phase densities than PA11. Such a result is expected and is usually ascribed to the shorter aliphatic chain of PA6 compared to PA11, which translates to a greater number of hydrogen bonds per unit mass and a more effective packing. Moreover, the calculated constrained amorphous phase density was higher than the free amorphous state valuefound in the literature [35] for both PA6 and PA11. The latter finding corroborates the assumption that the crystalline fraction alters the amorphous phase, reducing its free volume [19,45–47]. PA6I does not obey this rule, but the discrepancy can be attributed to the fact that the density calculation neglects the contribution of the impact modifier.

According to DSC analysis, the compression molded thin membranes show a similar value of mass degree of crystallinity, namely 0.24 for PA6,PA6I and 0.25 for PA11. The results for 2 mm PA6 and PA6I slabs were slightly different, but of the same order of magnitude. For the sake of completeness, the estimated melting peaks for the pristine slabs and the thin membranes are shown in Fig. 4a and b respectively.

Fig. 4a shows that among the pristine materials, only PA6 is characterized by a slightly bimodal distribution of the heat flow, while PA11 and PA6I exhibit a single sharp peak. On the other hand, all the thin membranes show a bimodal distribution of the heat flow. A partial overlapping of these two is evident for the PA6 and PA11 samples, whereas well-separated peaks are visible for the case of PA6I sample. In addition, while heat transfer in PA6 and PA11 occurs mainly at the higher temperature peak, the opposite is observed for the impact modified sample (PA6I). PA6 and PA6I have approximately the same melting temperature, with an average value corresponding to the greater melting peak around 220 °C (α crystal phase) [48,49], while PA11 exhibits a lower melting temperature (190 °C) that can be justified by the lower energetic contributions of hydrogen bonding per unit mass. Both values are in full agreement with literature values, which report melting temperatures of 220–230 °C and 190–195 °C for PA6 and PA11 respectively [50]. Finally, it was not possible to determine if the bimodal trends are due to the presence of two distinct crystalline phases (stable and metastable) or to a bimodal size distribution of the lamellae resulting from the hot pressing [51].

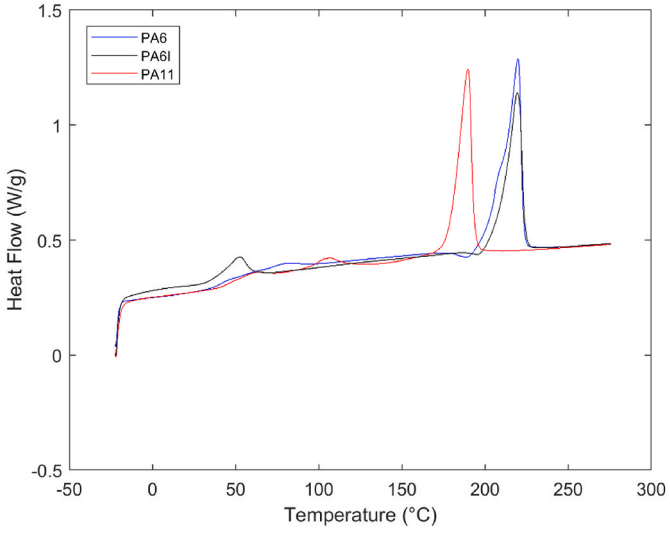

Fig. 4a. DSC peaks of supplied PA6 (blue), PA6I (black) slabs and PA11 pellet (red). (For interpretation of the references to colour in this figure legend, the reader is referred to the Web version of this article.)

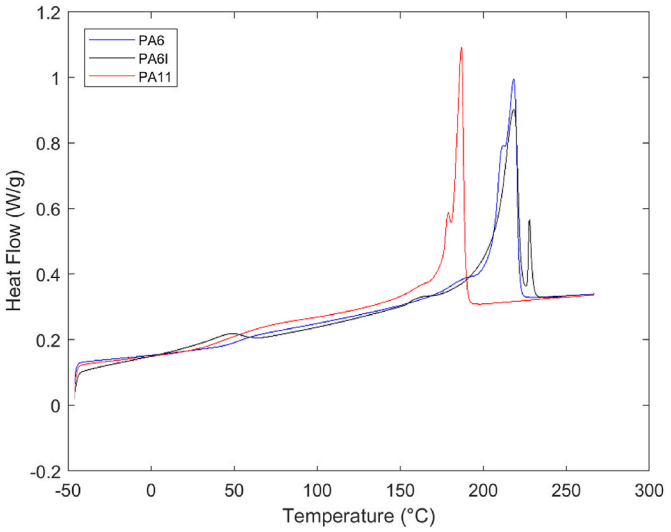

Fig. 4b. DSC peaks of thin membranes obtained through compression molding: PA6 (blue), PA11 (red) and PA6I (black). (For interpretation of the references to colour in this figure legend, the reader is referred to the Web version of this article.)

3.2. Permeation and sorption

As shown in Fig. 5, the isotherms measured using the ADVA apparatus for PA11 and PA6 followed Henry's law with good approximation.

Hydrogen sorption coefficients in PA11 and PA6 were evaluated as the slope of the interpolating lines, equal to 5.60×10^{-4} and 4.69×10^{-4} mol/(kg bar) respectively (0.0133 and 0.0120 $cm^3_{STP}/(cm^3$ bar)), with R^2 equal to 0.993 and 0.999. Hydrogen sorption kinetics is displayed in Fig. 6, where experimental data are shown together with the model fit.

The diffusion coefficient at 25 °C was estimated by fitting the transient data of the first pressure step reported in Fig. 6, obtaining 14.60×10^{-7} and 3.47×10^{-7} cm^2/s for PA11 and PA6 respectively. as this value does not change significantly with pressure in the range inspected. Finally, the permeability coefficients were estimated by means of the

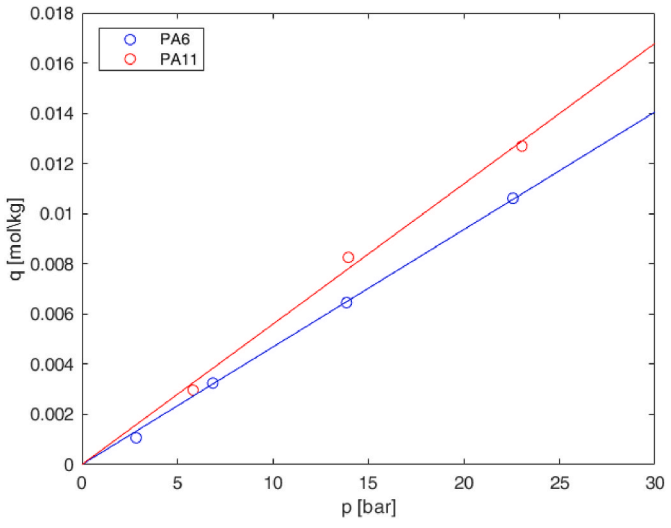

Fig. 5. Hydrogen sorption isotherms in PA11 (red) and PA6 (blue) at T = 25 °C, measured with ADVA equipment. (For interpretation of the references to colour in this figure legend, the reader is referred to the Web version of this article.)

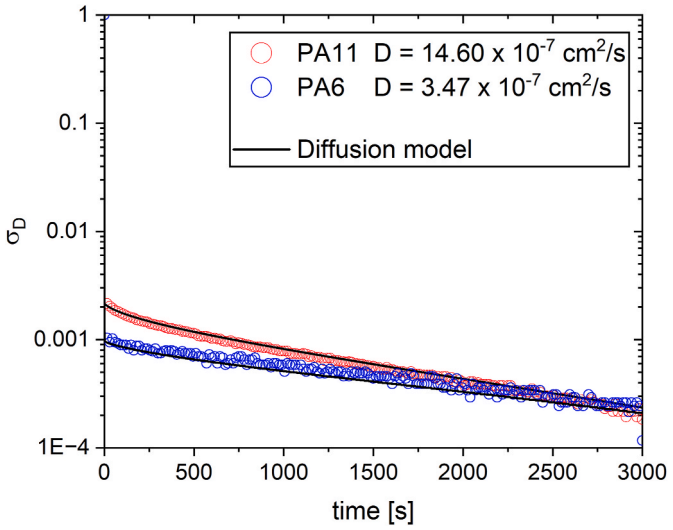

Fig. 6. Experimental hydrogen sorption kinetics in PA11 (red dots) and PA6 (blue dots) at T = 25 °C (first sorption point). (For interpretation of the references to colour in this figure legend, the reader is referred to the Web version of this article.)

solution-diffusion equation (Eq. (2)), to be 2.183 and 0.552 Barrer (1 Barrer = 10^{-10} cm^3_{STP}/(cm s cmHg)) for PA11 and PA6 respectively. The curves obtained with the permeation apparatuses are not reported, whereas the whole set of permeability, sorption, and diffusion coefficients data is summarized in Table 2. The corresponding plots of *P*, *D* and *S* as a function of T^{-1} are depicted in Figs. 7–9, respectively. Indeed, according to equations (3)–(5), such quantities are expected to exhibit an exponential dependence with T^{-1}: data at different temperatures obtained by the same lab and on the same sample were used to estimate permeation and diffusion activation energies, and enthalpy of sorption (Table 3).

As displayed in Fig. 7, the permeability of hydrogen in the compression molded PA6, PA6I and PA11 thin membranes measured at

Table 2
Comparison between the results obtained through hydrogen permeation and sorption tests in different polyamides samples with different geometries (compression molded membranes [C], injection molded plaques [I], pellets [P]) at different temperatures (20–80 °C) and pressures (6–700 bar).

Experimental Test	Sample	*T* [°C]	*p* [bar]	*P* [Barrer]	*D* [10^{-7} cm^2/s]	*S* [10^{-3} cm^3(STP)/(cm^3 bar)]
Permeation Test (UniBo)	PA6 C	20	6	0.24	1.88	9.57
		30		0.42	2.38	13.2
		40		0.68	3.61	14.1
		50		1.19	4.48	19.9
	PA6I C	20	6	0.56	2.47	17.0
		30		0.77	2.75	21.0
		40		1.06	3.69	21.5
		50		1.72	5.93	21.8
	PA11 C	20	6	0.97	4.86	15.0
		30		1.58	5.44	21.8
		40		2.47	9.81	18.9
		50		3.98	11.3	26.4
Permeation Test (TesTNet)	PA6 I	20	700	0.25	2.90	6.47
		55		0.57	–	–
		80		2.27	–	–
	PA6I I	20		0.39	3.40	8.60
		55		2.08	–	–
		80		8.44	–	–
Sorption Test (UoE)	PA6 P	25	23	0.55	3.47	12.0
	PA11 P	25	23	2.59	14.6	13.3

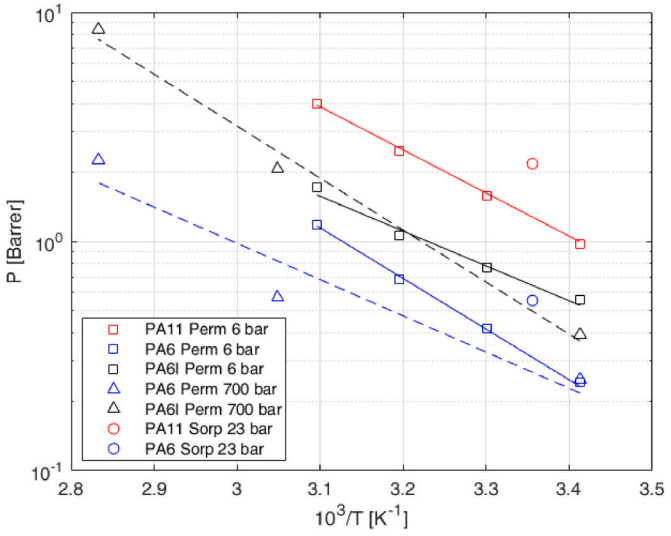

Fig. 7. Comparison of hydrogen permeability evaluated with different experimental techniques: "Perm 6 bar" experiments were carried out on PA6, PA6I and PA11 films at 6 bar between 20 and 50 °C; "Perm 700 bar" experiments were carried out on PA6 and PA6I slabs at 700 bar between 20 and 80 °C; "Sorp 23 bar" data show permeability evaluated as *DS* from sorption tests carried out on PA6 and PA11 pellet at 25 °C and pressures up to 23 bar.

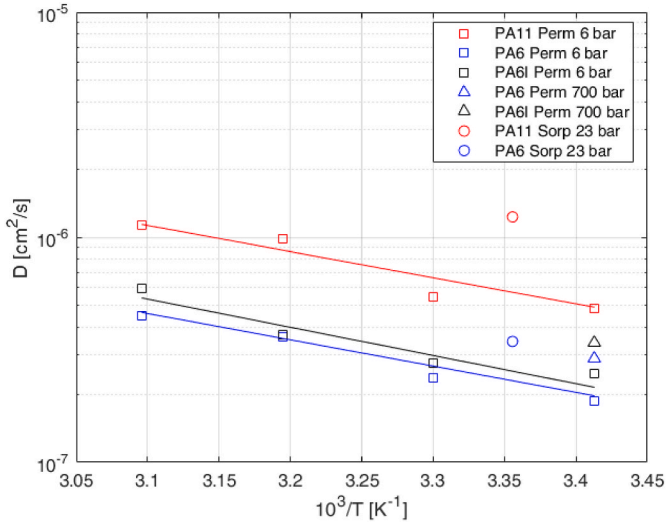

Fig. 8. Comparison of hydrogen diffusion coefficients evaluated with different experimental techniques. "Perm 6 bar" experiments were carried out on PA6, PA6I and PA11 membranes at 6 bar between 20 and 50 °C. "Perm 700 bar" experiments were carried out on PA6 and PA6I slabs at 700 bar and 20 °C. "Sorp 23 bar" tests were carried out on PA6 and PA11 pellet at 25 °C and pressures up to 23 bar.

6 bar follows an Arrhenius exponential law in all cases ($R^2 > 0.979$). The diffusion coefficients shown in Fig. 8 also respect the trend, but with slightly higher deviations ($R^2 > 0.924$) due to the higher error associated to the measurement of *D*, obtained from transient behavior. Finally, the sorption coefficient, which was estimated from the ratio of *P* and *D*, was impacted by the error propagation and thus the trends, shown in Fig. 9, especially for the case of PA6I and PA11, result in a worse linear regression ($R^2 > 0.706$).

3.3. Comparison between different materials and methods

The analysis of permeation data reported in Fig. 7 reveals the trend

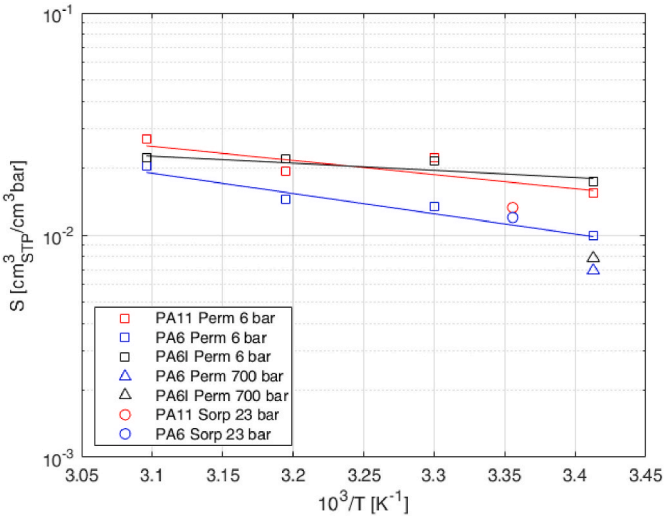

Fig. 9. Comparison of hydrogen solubility coefficients evaluated with different experimental techniques. "Perm 6 bar" experiments were carried out on PA6, PA6I and PA11 membranes at 6 bar between 20 and 50 °C. "Perm 700 bar" experiments were carried out on PA6 and PA6I slabs at 700 bar and 20 °C. "Sorp 23 bar" tests were carried out on PA6 and PA11 pellet at 25 °C and pressures up to 23 bar.

PA11 > PA6I > PA6 which is observed at all temperatures and is consistent with the density trend where PA6 > PA6I > PA11, considering that all the materials have similar crystalline degree (0.24–0.25). These results confirm the importance of the amorphous phase properties, as this is the region where the diffusion takes place. PA6 exhibits a lower permeability compared to PA11, in agreement with other literature references [25], and to PA6I, suggesting that the use of the impact resistance modifier in the latter material partially reduces the barrier performance of the polymer.

The high-pressure permeation tests carried out on PA6 and PA6I slabs produced by injection molding confirmed this trend. When analyzing the effect of pressure on the permeability, we observe that literature data reported in Table 3 generally indicate that at high pressure the permeability (and the diffusivity) is lower, presumably due to the lower polymer free volume available, and the activation energy of permeation is higher, which is also consistent with this explanation. Data obtained in this work on PA6I confirm this trend with pressure, as visible in Table 3.

The PA6 permeability data in this work are similar at low and high pressures, while the activation energies are lower at higher pressure: a discrepancy may arise from the different forming process, which leads to a different thickness, but also to a different microstructure and crystallinity. The thicker samples tested in the high pressure device are expected to be mainly characterized by bulk crystallized spherulites in the core, with a low fraction of oriented lamellae in the skin, which are predominant in thinner films. Thicker samples thus are expected to have a lower tortuosity with respect to thin films and less resistance to diffusion.

Apart from the thickness, also the different forming processes may lead to different microstructures and, consequently, permeability. The effect of different forming process on the hydrogen permeability in PA6 is clearly shown in Tables 3 and ie the compression molding (0.23 Barrer) leads to lower values with respect to extrusion (0.45 Barrer) and injection molding (1.45 Barrer).

The solubility of hydrogen in PA6 pellet directly measured in ADVA agrees with the values obtained indirectly through permeation experiments in the low-pressure range. On the other hand, for PA11, the direct method gives slightly lower values with respect to the indirect measurement. Concerning the diffusivity, higher values were calculated for PA6 and PA11 pellet used for the sorption tests, compared to PA6 and PA11 compression molded membranes used for the permeation measurements. As a result, also the permeability obtained indirectly, using the solution-diffusion equation is higher than the value identified from the low-pressure permeation test. The reason for such a discrepancy lies in the different crystalline morphology resulting from the material processing. While the pellet is produced through a stress-free bulk crystallization, during compression molding crystallization occurs with an applied stress hence leading to crystalline domains mainly oriented perpendicularly to the thickness and a higher tortuosity. It is important to note that the geometries of the samples analyzed in the two types of experiment are different, and the diffusion coefficient is consequently estimated with two different methodologies. The diffusion coefficient obtained via the time-lag method during a direct permeation test is affected by the path of molecules along the thickness direction. The biaxial extension during compression molding orients the crystallites in the directions perpendicular to the thickness, increasing the tortuosity along the same direction and lowering the measured diffusivity. On the other hand, in the sorption test on a pellet, the gas follows the radial direction of the pellet and encounters crystallites that are randomly oriented, experiencing a lower tortuosity compared to the case of thin membranes and a faster diffusion. Solubility is much less affected by the microstructure and the morphology of crystals, so that the data obtained from different techniques are in better agreement. The modest and comparable amount of crystallinity (0.24–0.25) calculated in PA6, PA6I and PA11 samples suggests that the amorphous phase controls the hydrogen transport properties. In particular, the higher hydrogen diffusion coefficient in PA11 compared to PA6 may derive from the greater free volume and lower density. On the other hand, the presence

Table 3
Activation energies of permeation and diffusion, and relative coefficients at 20 °C calculated from the best fitting of the experimental data obtained in this work (T.W.), compared to the literature references. The materials were produced using different processes (E: Extrusion; I: Injection Mold; IV: Cut from a type IV tank; L: Separated from laminated tube; C: Compression Mold).

Mat.	Ref	Proc.	p [bar]	P at 20 °C [Barrer]	E_p [kJ/mol]	D at 20 °C [10^7 cm^2/s]	E_D [kJ/mol]	T_{min} [°C]	T_{max} [°C]
PA	[23]	–	–	0.45	26			−10	30
PA6	[24]	E	132	0.45	30			−30	85
PA6	[9]	I	250	1.45	21.4			−15	85
PA6	[9]	I	350	0.76	22.6			−15	85
PA6	[9]	I	500	0.39	23.2			−15	85
PA6	[25]	IV	150	0.26	37.7	2.59	52.1	35	85
PA6	[25]	IV	437.5	0.16	41.7	2.21	34.8	35	85
PA6	[25]	IV	875	0.11	45.6	1.82	33.4	35	85
PA6	T.W.	C	6	0.23	41.2	1.83	23.8	20	40
PA6	T.W.	I	700	0.22	30.3	2.90		20	40
PA11	[28]	L	–	1.17	31.6	6.52	29.7	20	60
PA11	T.W.	C	6	0.99	36.8	4.54	24.6	20	40
PA6I	T.W.	C	6	0.53	29.0	2.23	22.8	20	40
PA6I	T.W.	I	700	0.37	43.5	3.40		20	40

of the less dense impact modifier in PA6I reduces significantly the overall density and PA6I has a higher hydrogen uptake and diffusion coefficient compared to the pristine PA6. As a consequence, PA6I has higher permeability with respect to PA6, showing that the high impact of solubility on the barrier performance, especially at low temperatures. The PA6 and PA11 sorption coefficients evaluated with ADVA equipment agree well with the ones from the low-pressure permeation tests, even though some underestimation is visible for the case of PA11. On the other hand, the sorption coefficient estimated from the permeation tests on the slabs at 700 bar are consistently lower and that may be attributed to the fact that the amorphous matrix free volume decreases with pressure. However, the diffusion coefficients obtained at high pressures on slabs are higher than the ones of the films in the low-pressure regime: such result indicates that the microstructure plays a relevant role in determining the diffusion coefficient, as the lower tortuosity in the slabs overcomes the effect of the free volume reduction resulting from the high pressure. While the free volume acts on both solubility and diffusivity, the tortuosity affects mostly the kinetic factors, namely the diffusivity, which is consistent with the observed results.

3.4. Activation energies

The activation energies of permeation and diffusion calculated in this work are summarized in Table 3, showing that all results lie between the ones reported in the literature by other authors. Different values arise from the different forming process, which ultimately should lead to negligible variations of crystallinity and thus solubility, but significant variations of final microstructure, which affect diffusivity and permeability.

Our results suggest that the activation energy of permeation for PA6 ranges between 41.2 and 30.3 kJ/mol, considering low- and high-pressure permeation tests respectively. Sun et *al.* [25] estimated lower values for injection molding samples, namely 21.4, 22.6 and 23.2 kJ/mol at pressures 250, 350, and 500 bar respectively in the temperature range −10 °C–85 °C. Humpenoder [23] calculated a value of 26 kJ/mol for a generic polyamide between −10° and 20 °C without specifying the forming process. The results presented in this work at 6 bar are consistent with the value of 30 kJ/mol reported by Smith et al. [23] at 132 bar which refers to an extruded PA6 sample, while the results at 700 bar are consistent with the one reported by Dong et al. [25], namely, 37.7, 41.7, and 45.6 kJ/mol at pressures 150, 440, and 870 bar respectively, in the range 30–80 °C. The same authors identified a diffusion activation energy of 48.3, 29.9, and 29.8 kJ/mol in the same conditions, which are higher than our results at 6 bar, equal to 23.8 kJ/mol. The enthalpy of sorption of PA6 has positive values (17.5 kJ/mol), as it was also observed by Dong et al. [25], at the same conditions, even if their values change sign with pressure namely, −14.4, 6.87, and 12.2 kJ/mol. No other data regarding activation energies of hydrogen in PA6 were found in the literature. The activation energy of permeation and diffusion in PA11 calculated in this work, 36.8 and 24.6 kJ/mol, is comparable with the findings of Ash et al. [28] who reported values of 31.6 and 29.7 kJ/mol. As a result, the enthalpy of sorption calculated in this work is equal to 12.2 kJ/mol, higher with respect to the one reported by the same authors (1.88 kJ/mol). The sorption heat behavior can be explained considering gas sorption as a two-step process which involves the condensation of the gas and the mixing of the condensed penetrant within the polymer phase. Consequently, the sorption enthalpy can be expressed as the sum of two contributions: the enthalpy of condensation (ΔH_{cond}) and the mixing enthalpy (ΔH_{mix}) which is related to the non-ideality of polymer–penetrant mixture:

$$\Delta H_S = \Delta H_{cond} + \Delta H_{mix} \quad \text{Eq. (15)}$$

The heat of condensation is always negative while the mixing enthalpy can be either positive or negative depending on the gas-polymer interactions. In general, the heat of condensation represents the main contribution, thus, gas sorption is commonly an exothermic phenomenon. However, for the gases with low critical temperature, a positive enthalpy of mixing may overcome the low heat of condensation thus leading to an endothermic process. Such a behavior has already been reported for hydrogen sorption in PA11 [23], LDPE [52] and PDMS [53].

3.5. Minimum thickness

To give a more comprehensive and intuitive description of the different expected performances of PA6 and PA6I tested samples as type IV tank liner materials, the minimum thickness required L_R to keep the leak per unit volume of the tank l_T within a given threshold has been calculated as proposed in Eq. (16):

$$L_R = \frac{P\,\Delta p\,A_T}{V_T l_T} \quad \text{Eq. (16)}$$

Where P is the hydrogen permeability measured at $\Delta p = 700$ bar and T = 20 °C, A_T is the surface area of the tank and V_T is the volume of the tank. The required mass of liner, therefore, is:

$$m = \rho_{SC}\,A_T\,L_R \quad \text{Eq. (17)}$$

Considering a cylindrical tank with a certain tank diameter D_T and length L_T, assuming a storage volume of $V_T = 249$ L (typical of a large car) with an aspect ratio $L_T/D_T = 2.8$, and using high pressure hydrogen permeability in PA6 (0.25 Barrer) and PA6I (0.39 Barrer) at 700 bar and 20 °C reported in Table 2, eq [16]. and eq [17]. lead to the trends reported in Fig. 10.

As displayed in the chart, the use of PA6 as liner material requires a smaller thickness and less mass to meet a given leak per unit volume compared to PA6I. In particular, the safety threshold of 6 cm^3(STP)/(h L) fixed by (EU) No 406/2010 [6,7] is accomplished using 2.01 kg (0.78 mm) of PA6 or, alternatively 3.14 kg (1.21 mm) of PA6I. Considering that the mass of hydrogen stored at T = 20 °C and 700 bar in the case study reservoir volume is approximately 10 kg, this translates in having a mass percentage of liner equal to 17 % and 24 % respectively, which outperforms the typical value of around 50–60 % characteristic of HDPE liner [54].

4. Conclusions

An experimental campaign on hydrogen permeability, sorption, and diffusion in PA6, PA11 and PA6I samples has been carried out using both sorption and direct permeation tests, leading to results in substantial agreement with each other and literature references, considering the deviation of the results caused by different hypothesized microstructures resulting from different thicknesses and forming technologies. Besides the experimental uncertainties, the discrepancy between the results obtained by the two techniques is expected to be ascribed mainly to the dependence of the diffusivity, i.e. the kinetics of the permeation process, to the crystalline morphology, which affects the tortuosity of the diffusive path. PA6 exhibited a permeability coefficient around three times lower than the one of PA11, and that is associated to its higher amorphous density. In general, some differences between data obtained with different techniques are due to the fact that the samples used have different shapes and have been obtained with different processes, and they thus have a different crystal morphology, e.g. powder or pellets versus films or slabs. In this respect, the sorption test is more versatile as it can be performed on any type of solid sample, while the permeation test is bound to the film/slab morphology to ensure isolation between the upstream and downstream side. The solubility value is less affected by microstructural differences with respect to diffusivity and permeability, as it is an equilibrium value independent of the time needed to reach it, and thus it does not depend on geometric factors such as tortuosity, but it can offer only an indirect estimate of permeability. It is observed, in this work as in previous ones, that hydrogen solubility

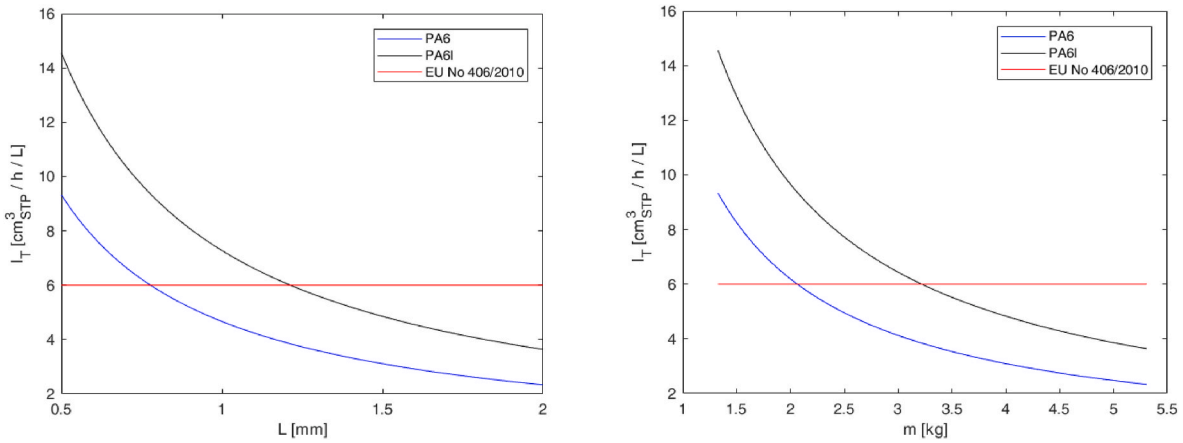

Fig. 10. Calculation of the hydrogen leak per unit volume of tank as function of liner thickness and mass for PA6 and PA6I, calculated using the experimental permeability results at 700 bar and 20 °C. Threshold set by (EU) 406/2010 [6].

increases with temperature, albeit slightly: such a behavior is not usual for gas sorption in polymers, but it has often been observed for hydrogen and other low critical temperature gases, and was explained considering its peculiar thermodynamic behavior. The presence of the impact modifier in PA6I led to a slightly lower barrier performance of the pristine PA6, which is substantially caused by the higher free volume of this material. Nevertheless, the slightly worse barrier performance of the PA6I sample is counterbalanced by its superior impact resistance which still makes it a promising alternative for high-pressure hydrogen storage type IV tanks. The threshold leak per unit volume set by EU regulations, in fact, can be met with a thickness of 1.2 mm which for the case study considered translates into the 24 % of total weight of the tank.

CRediT authorship contribution statement

Lorenzo Merlonghi: Writing – original draft, Methodology, Investigation, Formal analysis, Data curation. **Omar Atiq:** Writing – review & editing, Methodology, Investigation, Formal analysis, Data curation. **Riccardo Rea:** Writing – review & editing, Methodology, Formal analysis, Data curation. **Enzo Mangano:** Writing – review & editing, Supervision, Methodology. **Alexander Stroeks:** Writing – review & editing, Supervision, Resources, Methodology, Data curation. **Marco Giacinti Baschetti:** Writing – review & editing, Supervision, Project administration, Funding acquisition. **Maria Grazia De Angelis:** Writing – review & editing, Supervision, Project administration, Funding acquisition.

Declaration of competing interest

The authors declare that they have no known competing financial interests or personal relationships that could have appeared to influence the work reported in this paper.

Acknowledgments

This research forms part of the research program of DPI, project 844: *Modelling and Design of Multiphase Polymeric Materials for High Performance Applications Across Multiple Scales.*

References

[1] Rogers HC. Hydrogen embrittlement of metals. Science 1968;159:1057–64. https://doi.org/10.1126/science.159.3819.1057.
[2] Li X, Ma X, Zhang J, Akiyama E, Wang Y, Song X. Review of hydrogen embrittlement in metals: hydrogen diffusion, hydrogen characterization, hydrogen embrittlement mechanism and prevention. Acta Metall Sin 2020;33:759–73. https://doi.org/10.1007/s40195-020-01039-7.
[3] Su Y, Lv H, Zhou W, Zhang C. Review of the hydrogen permeability of the liner material of type iv on-board hydrogen storage tank. World Electric Vehicle Journal 2021;12:130. https://doi.org/10.3390/wevj12030130.
[4] Air A, Shamsuddoha M, Prusty BG. A review of Type V composite pressure vessels and automated fibre placement based manufacturing. Compos B Eng 2023;253:110573. https://doi.org/10.1016/j.compositesb.2023.110573.
[5] Ahluwalia RK, Hua TQ, Peng JK. On-board and Off-board performance of hydrogen storage options for light-duty vehicles. Int J Hydrogen Energy 2011;37:2891–910. https://doi.org/10.1016/j.ijhydene.2011.05.040.
[6] COMMISSION REGULATION (EU) No 406/2010 of 26 April 2010 implementing Regulation (EC) No 79/2009 of the European Parliament and of the Council on type-approval of hydrogen-powered motor vehicles. Off J Eur Union L 18.5.2010;122. p.1, http://data.europa.eu/eli/reg/2010/406/oj.
[7] Adams P, Bengaouer A, Cariteau B, Molkov V, Venetsanos AG. Allowable hydrogen permeation rate from road vehicles. Int J Hydrogen Energy 2011;36:2742–9. https://doi.org/10.1016/j.ijhydene.2010.04.161.
[8] Fujiwara H, Ono H, Ohyama K, Kasai M, Kaneko F, Nishimura S. Hydrogen permeation under high pressure conditions and the destruction of exposed polyethylene-property of polymeric materials for high-pressure hydrogen devices (2)-. Int J Hydrogen Energy 2021;46:11832–48. https://doi.org/10.1016/j.ijhydene.2020.12.223.
[9] Sun Y, Lv H, Zhou W, Zhang C. Research on hydrogen permeability of polyamide 6 as the liner material for type IV hydrogen storage tank. Int J Hydrogen Energy 2020;45:24980–90. https://doi.org/10.1016/j.ijhydene.2020.06.174.
[10] Quantum, Q-LITE® Hydrogen Tanks (n.d.). https://www.qtww.com/product/hydrogen/(accessed March 19, 2024).
[11] UBE corporation, Ube Industries Supplying Nylon 6 Resin for High-Pressure Hydrogen Tanks in Latest Toyota MIRAI Fuel Cell Vehicle (n.d.). https://www.ube.co.jp/ube/en/news/2020/20210303_01.html (accessed March 19, 2024).
[12] HEXAGON, Hydrogen Fuel Storage Systems (n.d.). https://hexagonpurus.com/our-solutions/hydrogen-systems/fuel-storage-systems (accessed March 19, 2024).
[13] Faurecia, Hydrogen Storage Systems (n.d.). https://www.faurecia.com/en/technologies/solutions-sustainable-mobility/zero-emission-solutions (accessed March 19, 2024).
[14] LUXFER, G-Stor® Go H2 Carbon Composite Type 4 Cylinders (n.d.). https://www.luxfercylinders.com/product/g-stor-go-h2-type-4-carbon-composite-cylinders/ (accessed March 19, 2024).
[15] Wijmans JGH, Baker RW. The solution – diffusion model: a unified approach to membrane permeation. In: Yampolskii Y, Pinnau I, Freeman BD, editors. Materials science of membranes for gas and vapor separation. John Wiley & Sons; 2006. https://doi.org/10.1002/047002903X.
[16] Müller-Plathe F. Towards a computational approach to penetrant diffusion in semicrystalline polymers. Chem Phys Lett 1991;177:527–35. https://doi.org/10.1016/0009-2614(91)90079-O.
[17] Sturm DR, Caputo KJ, Liu S, Danner RP. Diffusivity of solvents in semi-crystalline polyethylene using the Vrentas-Duda free-volume theory. J Polym Eng 2018;38:925–31. https://doi.org/10.1515/polyeng-2018-0047.
[18] Memari P, Lachet V, Rousseau B. Gas permeation in semicrystalline polyethylene as studied by molecular simulation and elastic model. Oil Gas Sci Technol 2015;70:227–35. https://doi.org/10.2516/ogst/2012074.
[19] Atiq O, Ricci E, Baschetti MG, De Angelis MG. Modelling solubility in semi-crystalline polymers: a critical comparative review. Fluid Phase Equil 2022;556:113412. https://doi.org/10.1016/j.fluid.2022.113412.
[20] Pokorny R, Seda L, Grof Z, Hajova H, Kosek J. Diffusion in semi-crystalline polymers. Computer Aided Chemical Engineering 2009;26:961–6. https://doi.org/10.1016/S1570-7946(09)70160-9.
[21] Nilsson F, Gedde UW, Hedenqvist MS. Penetrant diffusion in polyethylene spherulites assessed by a novel off-lattice Monte-Carlo technique. Eur Polym J 2009;45:3409–17. https://doi.org/10.1016/j.eurpolymj.2009.09.018.

[22] Kanesugi H, Ohyama K, Fujiwara H, Nishimura S. High-pressure hydrogen permeability model for crystalline polymers. Int J Hydrogen Energy 2023;48:723–39. https://doi.org/10.1016/j.ijhydene.2022.09.205.
[23] Humpenoder J. Gas permeation of fibre reinforced plastics. Cryogenics 1998;38:143–7. https://doi.org/10.1016/S0011-2275(97)00125-2.
[24] Baschetti MG, Minelli M. Test methods for the characterization of gas and vapor permeability in polymers for food packaging application : a review. Polym Test 2020. 2020. p. 106606. 89, https://doi.org/10.1016/j.polymertesting.2020.106606.
[25] Dong C, Liu Y, Li J, Bin G, Zhou C, Han W, Li X. Hydrogen permeability of polyamide 6 used as liner material for type IV on-board hydrogen storage cylinders. Polymers 2023;15:3715. https://doi.org/10.3390/polym15183715.
[26] Condé-Wolter J, Ruf MG, Liebsch A, Lebelt T, Koch I, Drechsler K, Gude M. Hydrogen permeability of thermoplastic composites and liner systems for future mobility applications. Composites Part A 2023;167:107446. https://doi.org/10.1016/j.compositesa.2023.107446.
[27] Picard E, Vermogen A, Gerard JF, Espuche E. Barrier properties of nylon 6-montmorillonite nanocomposite membranes prepared by melt blending: influence of the clay and dispersion state Consequences on modelling. J Membr Sci 2007;292:133–44. https://doi.org/10.1016/j.memsci.2007.01.030.
[28] Ash R, Barrer RM, Palmer DG. Solubility and transport of gases in nylon and polyethylene. Polymer 1970;11:421–35. https://doi.org/10.1016/0032-3861(70)90004-2.
[29] Smith B, Anovitz LM. Lifecycle verification of polymeric storage liners. Oak Ridge National Laboratories; 2013. https://doi.org/10.2172/1158738.
[30] Burgisi G, Paternoster M, Peduto N, Saraceno A. Toughness enhancement of polyamide 6 modified with different types of rubber: the influence of internal rubber cavitation. J Appl Polym Sci 1997;66:777–87. https://doi.org/10.1002/(SICI)1097-4628(19971024)66:4<777::AID-APP18>3.0.CO;2-O.
[31] Wunderlich B. Crystal melting. In: Macromolecular physics. New York: Academic Press; 1971. p. 70.
[32] Millot C, Fillot L-A, Lame O, Sotta P, Seguela R. Assessment of polyamide-6 crystallinity by DSC. J Therm Anal Calorim 2015;122:307–14. https://doi.org/10.1007/s10973-015-4670-5.
[33] Zhang Q, Mo Z, Liu S, Zhang H. Influence of annealing on structure of Nylon 11. Macromolecules 2000;33:5999–6005. https://doi.org/10.1021/ma000298d.
[34] Hughes SW. Archimedes revisited: a faster, better, cheaper method of accurately measuring the volume of small objects. Phys Educ 2005;40:468–74. https://doi.org/10.1088/0031-9120/40/5/008.
[35] van Krevelen DW. Properties of polymers. Third ed. Amsterdam: Elsevier Science; 1997.
[36] Brandrup J, Immergut EH. Polymer handbook. Third Edition. New York: John Wiley & Sons; 1989.
[37] Crank J. The mathematics of diffusion. second ed. Oxford: Clarendon Press, Oxford; 1975.
[38] Rea R, Tavitian A, Broom DP, et al. Validated methane adsorption isotherms up to 7.5 MPa on a reference Na-Y zeolite at near ambient temperatures. Adsorption 2024;30:1529–38. https://doi.org/10.1007/s10450-024-00518-y.
[39] Nguyen HGT, Sims CM, Toman B, Horn J, van Zee RD, Thommes M, Ahmad R, Denayer JFM, Baron GV, Napolitano E, Bielewski M, Mangano E, Brandani S, Broom DP, Benham MJ, Dailly A, Dreisbach F, Edubilli S, Gumma S, Möllmer J, N. H.. A reference high-pressure CH4 adsorption isotherm for zeolite Y: results of an interlaboratory study. Adsorption 2020;26:1253–66. https://doi.org/10.1007/s10450-020-00253-0.
[40] Wang JY, Mangano E, Brandani S, Brandani F, Pullumbi P. A novel adsorption differential volumetric apparatus to measure mass transfer in nanoporous materials. Sep Purif Technol 2022;283:120210. https://doi.org/10.1016/j.seppur.2021.120210.
[41] Kunz O, Wagner W. The GERG-2008 wide-range equation of state for natural gases and other mixtures: an expansion of GERG-2004. J Chem Eng Data 2012;57:3032–91. https://doi.org/10.1021/je300655b.
[42] Brandani S. Analysis of the piezometric method for the study of diffusion in microporous solids: Isothermal case. Adsorption 1998;4:17–24. https://doi.org/10.1023/A:1008831202564.
[43] Brandani S, Brandani F, Mangano E, Pullumbi P. Using a volumetric apparatus to identify and measure the mass transfer resistance in commercial adsorbents. Microporous Mesoporous Mater 2020;304:109277. https://doi.org/10.1016/j.micromeso.2019.01.015.
[44] Wang JY, Mangano E, Brandani S, Ruthven DM. A review of common practicesin gravimetric and volumetric adsorption kinetic experiments. Adsorption 2021;27:295–318. https://doi.org/10.1007/s10450-020-00276-7.
[45] Atiq O, Ricci E, Giacinti Baschetti M, De Angelis MG. Multi-scale modeling of gas solubility in semi-crystalline polymers: bridging Molecular Dynamics with Lattice Fluid Theory. Fluid Phase Equil 2023;570:113798. https://doi.org/10.1016/j.fluid.2023.113798.
[46] Memari P, Lachet V, Rousseau B. Molecular simulations of the solubility of gases in polyethylene below its melting temperature. Polymer 2010;51:4978–84. https://doi.org/10.1016/j.polymer.2010.08.020.
[47] Minelli M, De Angelis MG. An equation of state (EoS) based model for the fluid solubility in semicrystalline polymers. Fluid Phase Equil 2014;367:173–81. https://doi.org/10.1016/j.fluid.2014.01.024.
[48] Khanna YP, Kuhn WP. Measurement of crystalline index in nylons by DSC: complexities and recommendations. J Polym Sci B Polym Phys 1997;35:2219–31. https://doi.org/10.1002/(SICI)1099-0488(199710)35:14<2219::AID-POLB3>3.0.CO;2-R.
[49] Liu Y, Cui L, Guan F, Gao Y, Hedin NE, Zhu L, Fong H. Crystalline morphology and polymorphic phase transitions in electrospun nylon-6 nanofibers. Macromolecules 2007;40:6283–90. https://doi.org/10.1021/ma070039p.
[50] Walsh D, Zoller P. Standard pressure-volume-temperature data for polymers. Technomic, Lancaster; 1995.
[51] Ben Salem D, Pulpytel J, Pillier F, Pailleret A, Arefi-khonsari F. Amorphization and polymorphism modification of polyamide-6 films via open-air non-equilibrium atmospheric pressure plasma jet treatment. Plasma Process Polym 2014;11:961–73. https://doi.org/10.1002/ppap.201400030.
[52] Sun J, Wang H, Chen M, Ye J, Jiang B, Wang J, Yang Y, Ren C. Solubility measurement of hydrogen, ethylene, and 1-hexene in polyethylene films through an intelligent gravimetric analyzer. J Appl Polym Sci 2017;134:1–7. https://doi.org/10.1002/app.44507.
[53] Galizia M, Smith ZP, Sarti GC, Freeman BD, Paul DR. Predictive calculation of hydrogen and helium solubility in glassy and rubbery polymers. J Membr Sci 2015;475:110–21. https://doi.org/10.1016/j.memsci.2014.10.009.
[54] Hua TQ, Roh H, Ahluwalia RK. Performance assessment of 700-bar compressed hydrogen storage for light duty fuel cell vehicles. Int J Hydrogen Energy 2017;42:25121–9. https://doi.org/10.1016/j.ijhydene.2017.08.123.